CrossMark

J. Fluid Mech. (2018), *vol.* 836, *pp.* 222–237. © Cambridge University Press 2017
doi:10.1017/jfm.2017.803

Implication of Taylor's hypothesis on measuring flow modulation

X. I. A. Yang[1] **and M. F. Howland**[1,†]

[1]Center for Turbulence Research, Stanford University, Stanford, CA 94305, USA

(Received 15 May 2017; revised 29 October 2017; accepted 1 November 2017;
first published online 11 December 2017)

A convective velocity must be specified when using Taylor's frozen eddy hypothesis to relate temporal and spatial fluctuations. Depending on the quantity of interest, using different convective velocities (i.e. time-mean velocity, global convective velocity, etc.) may lead to different conclusions. Often, using Taylor's hypothesis, the relation between temporal and spatial fluctuations is simplified by assuming a temporally averaged velocity as the convection velocity. In flows where turbulence fluctuations are much smaller than the mean flow velocity, the above treatment does not bring in much error (at least for short periods of time). However, when turbulence fluctuations are comparable to the mean velocity, using a constant convective velocity for fluid motions of all scales can sometimes be problematic. In the context of wall-bounded flows, turbulence fluctuations are comparable to the mean flow in the near-wall region, and as a result, using a constant global convective velocity for converting temporal signals to spatial ones distorts the spatial eddies. Although such distortion will not significantly affect measurements of flow quantities including central moments and power spectra, the significance of amplitude modulation is largely overestimated. Here, we show that if temporal hot-wire data are to be used for studying spatial amplitude modulation, the local fluid velocity must be used as the local convective velocity. The impact of amplitude modulation on power spectra and skewness are reconsidered using the proposed correction.

Key words: turbulence modelling, turbulence theory, turbulent boundary layers

1. Introduction

Amplitude modulation in wall-bounded flows refers to a nonlinear inter-scale interaction where the amplitude of small-scale fluid motions is modulated by large-scale fluid motions (Rao, Narasimha & Narayanan 1971; Bandyopadhyay & Hussain 1984; Hutchins & Marusic 2007). As a generic example of amplitude modulation, let us consider a large-scale signal ϕ_L and a small-scale signal ψ_S. Here, ϕ_L is the modulating signal and ψ_S is the modulated signal. Following Mathis, Hutchins & Marusic (2009*a*), the amplitude modulation may be quantified as follows:

$$R \equiv \frac{\langle \phi_L \cdot \mathrm{env}_L(\psi_S) \rangle}{\mathrm{STD}(\phi_L) \cdot \mathrm{STD}(\mathrm{env}_L(\psi_S))}, \tag{1.1}$$

† Email address for correspondence: mhowland@stanford.edu

https://doi.org/10.1017/jfm.2017.803 Published online by Cambridge University Press

where the subscripts L and S denote the large-scale and the small-scale components of the signal respectively. The standard deviation and the envelope of a signal are denoted as STD$(\cdot)$ and env$(\cdot)$ respectively. In the context of wall-bounded flows, the modulating signal is usually the large-scale streamwise velocity fluctuation. The modulated signal is usually the small-scale streamwise velocity fluctuation (for other modulated signals see Talluru *et al.* 2014). Hereafter, we will refer to one-dimensional temporal or spatial velocity fluctuation data as signals. The large- and small-scale motions differ in their characteristic length scales. Fluid motions whose characteristic length scales are greater than a pre-defined length scale l are large-scale motions and the small-scale motions are the complement (see e.g. Hutchins & Marusic 2007; Mathis *et al.* 2009*a*). The length scale l is selected such that the small scales are responsible for the 'inner peak' in the velocity power spectrum, and the large scales are responsible for the so-called 'outer peak' (Hutchins & Marusic 2007; Mathis *et al.* 2009*a*). Since the 'outer peak' is only separated from the 'inner peak' at friction Reynolds numbers larger than $O(10^3)$ (Hutchins & Marusic 2007), an l that separates the 'inner peak' from the 'outer peak' only exists at high Reynolds numbers. Due to the inability to define l at low and moderate Reynolds numbers, the process of amplitude modulation is formally only present in flows at high Reynolds numbers. Hutchins & Marusic (2007) and Mathis *et al.* (2009*a*) used $l = C\delta$, where δ is an outer length scale and C is an $O(1)$ constant. Later, Mathis, Hutchins & Marusic (2011*a*), Ganapathisubramani *et al.* (2012) and Baars *et al.* (2015) used $l^+ = 7000$ (where $+$ indicates normalization by wall units). The strength of amplitude modulation (i.e. R) depends only weakly on l (Mathis *et al.* 2011*a*). $R \approx 0.7$ in the viscous sub-layer. In the log region $R \approx 0$, and the measured R is often negative in the bulk region (see detailed discussion of this behaviour in Baars, Hutchins & Marusic 2017). This behaviour is found in boundary layer, channel, and pipe flows with the measured R collapsing at matched friction Reynolds numbers (Mathis *et al.* 2009*b*). R was also found to increase as a function of the Reynolds number (Mathis *et al.* 2009*a*).

It is worth noting that (1.1) lacks generality in its measure of amplitude modulation (Schlatter & Örlü 2010). More generally, the presence of amplitude modulation must be examined by conditioning small-scale signals based on large-scale signals (Ganapathisubramani *et al.* 2012; Agostini & Leschziner 2014). However, since the presence of amplitude modulation in wall-bounded flows is now well established, equation (1.1) suffices as a description of the phenomenon (Baars *et al.* 2017).

In addition to (1.1), the significance of amplitude modulation can also be assessed by comparing the small-scale velocity signal u'_S and the de-modulated velocity signal u^*,

$$u^* = \frac{u'_S}{1 + \beta u'_L}, \tag{1.2}$$

where β is such that $\langle \mathrm{env}_L(u^*) \cdot u'_L \rangle = 0$ and $u' = u'_S + u'_L$. Amplitude modulation is strong if the de-modulated small-scale signal u^* differs from the original small-scale signal u'_S. Conversely, amplitude modulation is weak if the two signals are similar. The de-modulated signal can be used in the predictive inner–outer model

$$u'_m = u^*(1 + \beta u'_L) + \alpha u'_L, \tag{1.3}$$

where u'_m is the modelled signal (containing both the large-scale and the small-scale contents) and α is an $O(1)$ constant (see Marusic, Mathis & Hutchins 2010; Mathis *et al.* 2011*a*). Although only indirectly, the usefulness of amplitude modulation may also be assessed by comparing the modelled full signal u'_m and the original full signal

https://doi.org/10.1017/jfm.2017.803 Published online by Cambridge University Press

u' (see e.g. Mathis *et al.* 2011*a*, 2013). Equation (1.3) is supposedly validated if the statistics of the modelled signal agree with the statistics of the original signal. However, comparing u'_m and u' assesses both the modelled superposition effects of large-scale and small-scale velocities in the near-wall region (Yang, Marusic & Meneveau 2016*a*,*b*; Yang *et al.* 2016*c*) and the modelled amplitude modulation effects. To focus on the amplitude modulation process alone, in later sections, we will compare u^* and u'_S.

Aside from the amplitude modulation, frequency modulation was quantified in Ganapathisubramani *et al.* (2012) by considering zero crossings of small-scale signals and later in Baars *et al.* (2015) using wavelets. In this work, we will focus on amplitude modulation, although it is likely that the effects of Taylor's hypothesis will be relevant to frequency modulation as well.

Amplitude modulation is most significant in the near-wall region at high Reynolds numbers. However, acquiring near-wall data at high Reynolds numbers poses challenges to currently available computational tools and measurement techniques. At high Reynolds numbers ($Re_\tau \sim O(10^4)$), direct numerical simulations (DNS) and wall-resolved large-eddy simulations (LES) are prohibitively expensive (Choi & Moin 2012). The less computationally demanding approach of wall-modelled LES (WMLES), on the other hand, does not resolve the near-wall region (Piomelli & Balaras 2002) where the amplitude modulation is most significant. Therefore, previous investigations have mostly relied on hot-wire (HW) anemometry experimental measurements. The study of spatial amplitude modulation has so far relied on temporal data which must be converted to the spatial domain by invoking Taylor's frozen turbulence hypothesis.

The use of Taylor's hypothesis has a long history (Taylor 1938) and warnings against the uncritical use of this hypothesis often appear in the literature (see e.g. Geng *et al.* 2015). Strictly speaking, the mean fluid convective velocity must be derived from the space–time correlation and is generally a function of the wall-normal distance (Kim & Hussain 1993) and the scales of the fluid motions (Del Álamo & Jiménez 2009). Depending on the quantities of interest, e.g. the topology of coherent structures, the power spectra, etc., using a bulk convective velocity across the entire boundary layer or a wall-normal-dependent convective velocity may yield varying conclusions (see e.g. Zaman & Hussain 1981; Lozano-Durán & Jiménez 2014*b*). Although the validity of Taylor's hypothesis is often challenged (e.g. Moin 2009), for many purposes, including measuring the power spectrum and the central moments, assuming frozen turbulence is in fact not problematic (see recent work by Squire *et al.* 2017). However, the applicability of Taylor's hypothesis in characterizing spectra and central moments does not adequately affirm its efficacy for quantifying amplitude modulation. Amplitude modulation's characterization depends not just on capturing the energy content at each wavenumber but also on capturing the phase information.

Directly examining the effects of Taylor's hypothesis on the quantification of spatial amplitude modulation requires spatial measurements that extend tens of boundary layer heights in the flow direction. This can be difficult in a laboratory set-up because the extent of experimental spatial data (obtained using techniques such as particle image velocimetry) typically do not exceed several boundary layer heights (see e.g. Doron *et al.* 2001; Squire *et al.* 2017). As an alternative, here, we use spatial data from DNS of channel flow and temporal HW data from boundary layer experiments at similar friction Reynolds numbers ($Re_\tau = u_\tau \delta/\nu$, where $u_\tau \equiv \sqrt{\tau_w/\rho}$ is the friction velocity, τ_w is the wall shear stress, ρ is the density, δ is the boundary layer height and ν is the kinematic viscosity). This is warranted for amplitude modulation analysis because

https://doi.org/10.1017/jfm.2017.803 Published online by Cambridge University Press

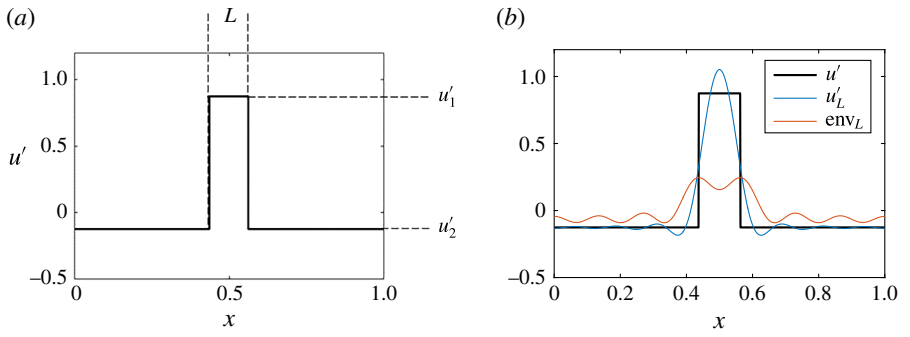


FIGURE 1. (Colour online) (*a*) A square velocity signal. The signal extends from 0 to 1 (normalization is arbitrary). $\langle u' \rangle = 0$. The square is of width L and is at $u' = u'_1$. The remainder of the signal is at $u' = u'_2$. (*b*) u', u'_L, and $\mathrm{env}_L(u'_S)$. R is the correlation between $\mathrm{env}_L(u'_S)$ and u'_L. Here a Fourier filter is used and the filtering length scale is $l = 0.125$.

R collapses for those two flow configurations at matched friction Reynolds numbers in the near-wall region (Mathis *et al.* 2009*b*).

The remainder of the article is organized as follows: in § 2, the effects of Taylor's hypothesis on velocity signals are illustrated using a square test signal and the one-dimensional advection-diffusion equation. Then, time varying convective velocities are used in place of a global constant convective velocity. These results are discussed in § 3, followed by a reassessment of amplitude modulation using the various metrics reviewed in this section. Since temporal and spatial amplitude modulation are not necessarily the same, we will repeat some previous analyses for spatial modulation. These re-analyses will be done for temporal data using the proposed conversion scheme and for spatial data. Concluding remarks are given in § 4.

2. Effects of Taylor's hypothesis

Here, we use two simplified cases to show that the spatial amplitude modulation is over-estimated when temporal signals are converted to space using Taylor's hypothesis.

2.1. *A square signal*

In this section, we will show that Taylor's hypothesis leads to signal distortion. To demonstrate such distortion, we will first consider a one-dimensional (1-D) square spatial signal (figure 1). We assume the signal is advected at its local velocity $u_c = u_o + u'$, where u_o is the mean. The global convective velocity of this signal is $u_c = u_o$. For now, let us assume the square shape of the signal is frozen. The plateau travels at a speed of $u_o + u'_1$ and the remainder of the signal travels at a speed of $u_o + u'_2$. By placing a probe at an arbitrary x location, we can measure the time it will take for the signal to pass the probe. The time it takes to pass the probe is $t_1 = L/(u_o + u'_1)$ and $t_2 = (1 - L)/(u_o + u'_2)$ for the plateau and the rest of the signal respectively. When converting the recorded temporal signal to a spatial one using a global convective velocity u_o, the width of the square-shaped plateau reduces because $t_1/t_2 = L/(1 - L) \cdot (u_o + u'_2)/(u_o + u'_1) < L/(1 - L)$. Hence, using Taylor's hypothesis to convert temporal signals to spatial ones does not recover the original spatial signal. Instead, using a constant convective velocity compresses regions where $u' > 0$ and stretches regions where $u' < 0$. For signals where $u_o \gg u'$, $(u_o + u'_2)/(u_o + u'_1) \approx 1$ and

https://doi.org/10.1017/jfm.2017.803 Published online by Cambridge University Press

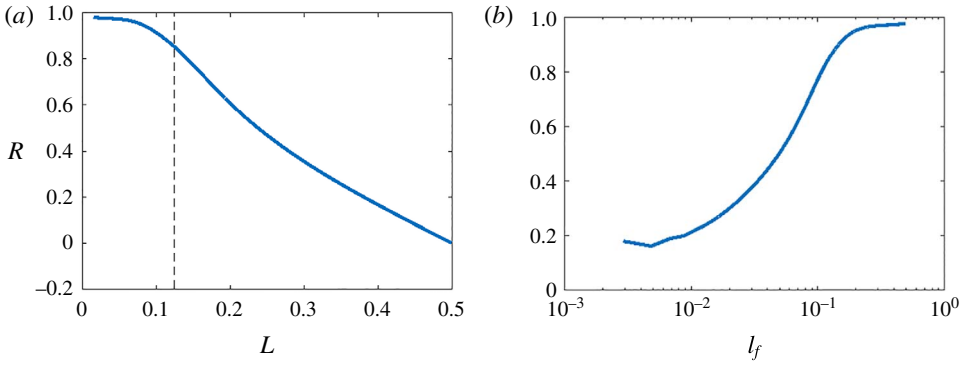


FIGURE 2. (Colour online) (*a*) Amplitude modulation R as a function of the square width L. The filtering length scale is fixed at $l = 0.125$ and is indicated using the dashed line. (*b*) R as a function of the filtering length scale. The width of the square is fixed at $L = 0.125$. The top-hat filter in physical space is used. Using the top-hat filter in Fourier space yields similar results (not shown). The square signal is assumed to be periodic.

this stretching is negligible; however, for signals where u_o is comparable to u', this distortion can be significant.

For wall-bounded flows, at a fixed y^+, $\langle u^+ \rangle$ is nearly Re_τ independent according to the law of the wall (see Hultmark *et al.* 2012; Marusic *et al.* 2013) whereas $\langle u'^{+2} \rangle$ is an increasing function of the Reynolds number (Hutchins & Marusic 2007). Therefore at high Reynolds numbers, STD(u') becomes comparable to $\langle u \rangle$ in the near-wall region, and the above-mentioned stretching effect will be significant.

Next, we consider the effect of this stretching on amplitude modulation. In order to illustrate the distortion's effect on amplitude modulation, we have measured R as functions of L (the square width) and l (filtering length scale) in figure 2. The exact magnitude of amplitude modulation is not relevant here but the trend is important. R is generally a decreasing function of L and an increasing function of l. Considering the above-mentioned stretching effect, R being an decreasing function of L suggests that using a global convective velocity leads to an over-estimated R. In addition, figure 2(*b*) confirms the expectation that R is an increasing function of l (Mathis *et al.* 2009*a*). These results are consistent with other simple wave forms (e.g. triangular, not shown).

2.2. *One-dimensional advection-diffusion equation*

We will now extend our discussion and consider the effects of Taylor's hypothesis on amplitude modulation for the 1-D advection-diffusion system. This system is formally similar to the Navier–Stokes equations. Here, the observations of § 2.1 will be tested on a broadband signal. Equation (2.1) is the 1-D advection-diffusion equation in its non-conservative form.

$$\frac{\partial u'}{\partial t} + (u_c + u')\frac{\partial u'}{\partial x} = \nu \frac{\partial^2 u'}{\partial x^2} + f, \tag{2.1}$$

where the mean convective velocity u_c is specified and kept constant, ν is the kinematic viscosity and f is a forcing. Two convective velocities $u_c = 1$ and 3 are used. The forcing is white both in time and in space and follows a uniform distribution from $-f_o$ to f_o. In order to ensure only the fluctuations are computed, after each time step, u' is de-trended by subtracting its mean. The computational

https://doi.org/10.1017/jfm.2017.803 Published online by Cambridge University Press

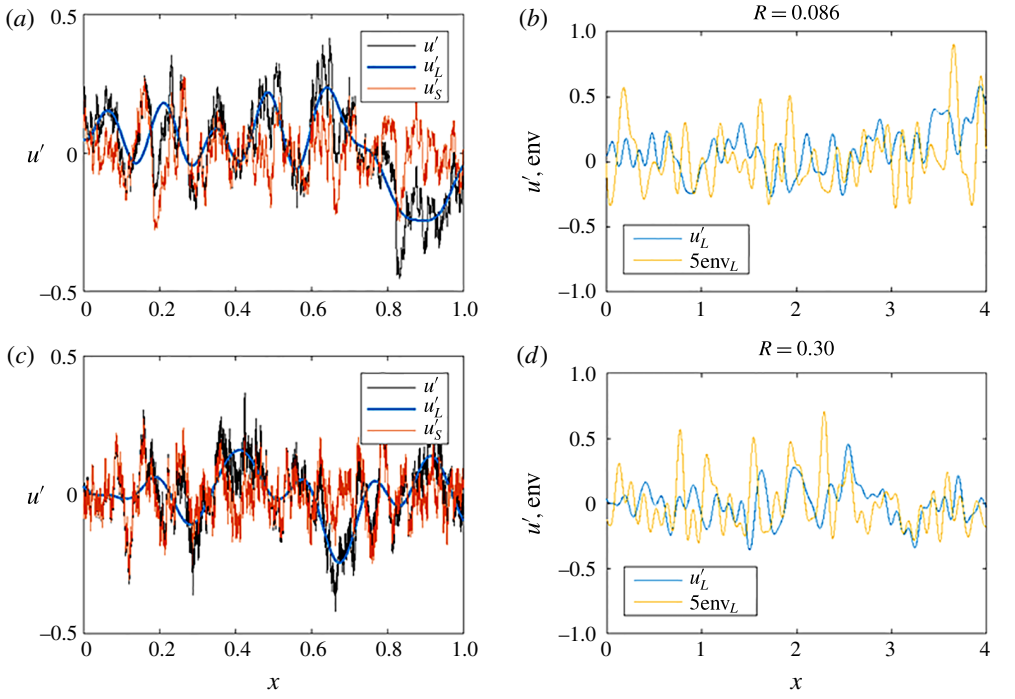


FIGURE 3. (Colour online) Sample signals from the $u_c = 1$ case. (*a*) Spatial signals u', u'_L and u'_S as functions of the spatial coordinate x. (*b*) u'_L and $\text{env}_L(u'_S)$. The large-scale component of the envelope of the small-scale component is amplified by a factor of 5 for better visualization. (*c*) Same as (*a*) but for the signal from virtual probes converted to space using Taylor's hypothesis. The convective velocity is specified: $u_c = 1$. (*d*) Same as (*b*) but for the signal from virtual probes converted to space using Taylor's hypothesis. The averaged amplitude modulation is $R = 0.086$ based on the spatial signal. The temporal signal, on the other hand, yields $R = 0.30$.

domain is of size L_x. Periodic conditions are imposed on both ends of the domain. The domain Péclet numbers are $Pe = u_c L_x/\nu \approx 3.3 \times 10^4$ and 9.8×10^4 for the $u_c = 1$ and $u_c = 3$ cases respectively. The domain Péclet number based on the forcing strength is $Pe_f = \sqrt{f_o L_x^3}/\nu = 3.25 \times 10^6$. We will study the effect of $\text{STD}(u')/\langle u \rangle$ for its typical values in the buffer layer and in the log region. The particular Pe and Pe_f are thus chosen. A second-order central finite difference scheme is used for both the advection term and the diffusion term. The one-dimensional computational domain is discretized uniformly with $\mathrm{d}x/L_x = 1/2^{15}$. Explicit Euler is used for time advancing. The time step size is such that the Courant–Friedrichs–Lewy (CFL) number is kept unchanged between the two cases (CFL = 0.3). The system reaches a statistically stationary state rapidly (in less than $5L_x/u_c$) and is simulated for $T \approx 100L_x/u_c$ to gather statistics. Temporal signals are recorded at 100 evenly spaced virtual probes across the computational domain. Spatial signals are directly available. For the amplitude modulation analysis, a top-hat filter in Fourier space is used for extracting large-scale features and the filtering length scale is $l/L_x = 1/2^8$ ($l/\mathrm{d}x = 2^7$). The viscous scale of this one-dimensional problem is $l_v = (\nu^2/f_o)^{1/3} \approx 1.5\,\mathrm{d}x$. The filtering length scale is such that $l \gg l_v$.

https://doi.org/10.1017/jfm.2017.803 Published online by Cambridge University Press

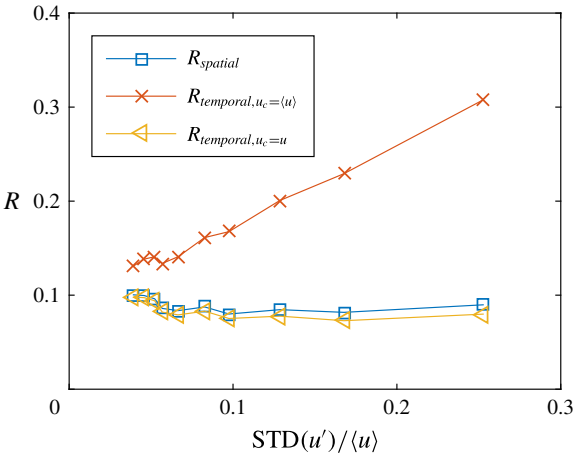


FIGURE 4. (Colour online) Measured R as a function of $\mathrm{STD}(u')/\langle u\rangle$. The spatial signals are used for $R_{spatial}$. The temporal signals are used for $R_{temporal,u_c=\langle u\rangle}$ and $R_{temporal,u_c=u}$, where the mean velocity and the local instantaneous velocity are used for the convective velocity respectively.

Figure 3 shows samples of u', u'_L, u'_S and $\mathrm{env}_L(u'_S)$ as functions of the spatial coordinate for the $u_c = 1$ case (for the temporal signal, Taylor's hypothesis is invoked to convert the signal from the temporal domain to the spatial domain). Results for the $u_c = 3$ case are similar, and are not shown for brevity. We can make a few observations. First, for both convective velocities, the amplitude modulation measured using the spatial signals is $R \approx 0.086$. We thus confirm that the amplitude modulation is not a function of the global convective velocity (by Galilean invariance). Second, by comparing figures 3(*b*) and 3(*d*), it is clear that Taylor's frozen turbulence hypothesis leads to over-estimated spatial amplitude modulation, which aligns with the observations in § 2.1. Third, amplitude modulation coefficients measured using temporal data (invoking Taylor's hypothesis) are $R = 0.3$ and 0.13 for the $u_c = 1$ and $u_c = 3$ cases respectively. Therefore, we can conclude that although amplitude modulation is over-estimated when Taylor's hypothesis is invoked, the estimate becomes more accurate when the ratio $\mathrm{STD}(u')/u_c$ decreases.

In figure 4, we show the effect of $\mathrm{STD}(u')/\langle u\rangle$ on R by varying the convective velocity in (2.1) while keeping the forcing and $\mathrm{d}t \cdot u_c$ unchanged. The system is under the same white forcing by keeping $\mathrm{d}t \cdot u_c$ constant. As the fluctuation to mean ratio increases, we expect an increasing amount of error when using Taylor's hypothesis. A few observations can be made. First, because we vary only the convective velocity, $R_{spatial}$ remains almost constant as $\mathrm{STD}(u')/\langle u\rangle$ increases because of the Galilean invariance. Second, invoking Taylor's hypothesis, $R_{temporal,u_c=\langle u\rangle}$ deviates from $R_{spatial}$ as $\mathrm{STD}(u')/\langle u\rangle$ increases. Using the local instantaneous velocity u as the convective velocity will be discussed in detail in § 3. As is clear from figure 4, when the local velocity is used as the convective velocity the spatial amplitude modulation is measured correctly using temporal data. Last, from figure 4, we may conclude that $\mathrm{STD}(u')/\langle u\rangle$ should be smaller than 0.05 for Taylor's hypothesis to be used for amplitude modulation analysis. For $\mathrm{STD}(u')/\langle u\rangle < 0.05$, the measured R using Taylor's hypothesis ($R_{temporal,u_c=\langle u\rangle}$) is no more than 20 % higher than $R_{spatial}$.

Figure 5 shows the power spectra computed using the spatial and the temporal signals for the case $u_c = 1$. The power spectrum of the spatial signal obtained by

https://doi.org/10.1017/jfm.2017.803 Published online by Cambridge University Press

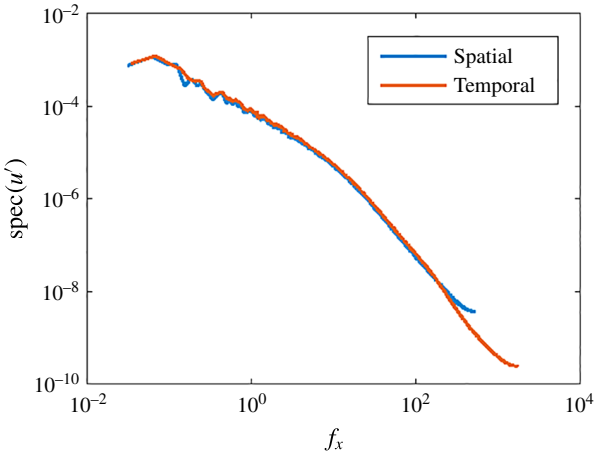


FIGURE 5. (Colour online) Power spectra computed using the spatial signal ('spatial') and the converted spatial signal using Taylor's hypothesis ('temporal') for the $u_c = 1$ case. spec(·) computes the power spectrum of the bracketed signal. The resolution of the spatial data is dx and the resolution of the temporal data is $u_c \cdot \mathrm{d}t = 0.3\,\mathrm{d}x$, resulting in the discrepancy at the tails.

converting the temporal signal to space using Taylor's hypothesis collapses with the power spectrum of the real spatial signal. However, the amplitude modulation process is approximately two times as strong for the converted spatial signal compared to the real spatial signal. Therefore, despite the observed collapse of the power spectra for spatial and temporal data, the spatial amplitude modulation is incorrectly measured if Taylor's hypothesis is invoked.

The fluctuation to mean ratio $\mathrm{STD}(u')/u_c \approx 0.25$ for the $u_c = 1$ case and ≈ 0.08 for the $u_c = 3$ case. This ratio is $\approx 0.2 \sim 0.3$ in the buffer layer and is ≈ 0.1 in the log region at friction Reynolds numbers $Re_\tau \sim O(10^3 - 10^4)$. For a given 1-D signal, the difference between spatial and temporal amplitude modulation is mostly a function of $\mathrm{STD}(u')/\langle u \rangle$. Therefore, a comparable amount of over-estimation of the spatial amplitude modulation (up to 200 %) is expected in those wall-normal regions when Taylor's hypothesis is invoked.

It is worth noting that the resulting signals in both cases are not skewed ($\langle u'^3 \rangle \approx 0$), therefore the measured R is an unambiguous measure of the amplitude modulation (Schlatter & Örlü 2010). The fact that $R \neq 0$ suggests that the 1-D advection-diffusion equation promotes nonlinear interactions among motions of different scales. Although this falls out of the scope of this work, the one-dimensional advection-diffusion equation may be exploited to investigate the mechanism behind the amplitude modulation.

3. Reassessment of hot-wire signals

In § 2, we showed that invoking Taylor's hypothesis leads to over-estimated spatial amplitude modulation using simplified examples. In this section, we demonstrate that this over-estimation of amplitude modulation is present in real-world fluid flows. Figure 6 shows the measured amplitude modulation R as a function of the wall-normal distance y^+ for DNS of channel flow at three Reynolds numbers, $Re_\tau = 950$, 2000 and

https://doi.org/10.1017/jfm.2017.803 Published online by Cambridge University Press

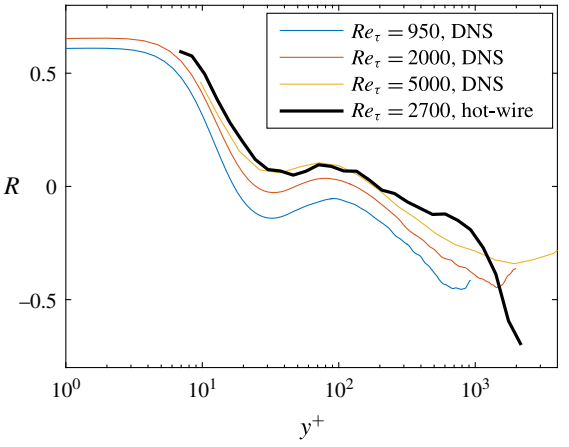


FIGURE 6. (Colour online) R as a function of the wall-normal distance. Results for $Re_\tau = 950$, 2000 and 5200 are from DNS of channel flow (Del Alamo *et al.* 2004; Hoyas & Jiménez 2006; Lee & Moser 2015; Lozano-Durán & Jiménez 2014*a*). $Re_\tau = 2700$ is HW data of a boundary layer.

5200 and for HW measurements of a boundary layer at $Re_\tau = 2700$. The temporal HW signals are converted to spatial ones using the frozen turbulence hypothesis. The DNS computational domain extends $8\pi\delta$ in the streamwise direction. Other details of the DNS can be found in Del Alamo *et al.* (2004), Hoyas & Jiménez (2006), Lee, Malaya & Moser (2013) and Lee & Moser (2015); the experimental set-up is detailed in Hutchins *et al.* (2009) and Talluru *et al.* (2014). The filtering length scale is $l^+ = 4000$ and a top-hat filter in Fourier space is used to separate the large-scale and the small-scale components. Within the limited range of moderate Reynolds numbers, the amplitude modulation is an increasing function of the Reynolds number (see also Mathis *et al.* 2009*a*). Figure 6 shows that amplitude modulation measured using HW data at $Re_\tau = 2700$, which is expected to be very similar to the $Re_\tau = 2000$ DNS, is in fact closer to the $Re_\tau = 5200$ DNS results, suggesting that spatial amplitude modulation may have been over-estimated when Taylor's hypothesis is used.

In § 3.1, we propose a new scheme to convert temporal data to space; instead of using the mean velocity as the convective velocity, the local fluid velocity is used. In § 3.2, the proposed methodology is used to re-analyse the hot-wire data. We will repeat a few analyses done by Mathis, Marusic and co-authors to quantitatively examine the difference between the temporal amplitude modulation process and the spatial amplitude modulation process. In § 3.3, we present a physical justification for the use of the local fluid velocity as the convective velocity.

3.1. *Local convective velocity*

Let us consider a one-dimensional temporal signal (e.g. a HW signal). As we have briefly discussed in § 2.1, in regions where $u' < 0$, the signal is stretched if the mean velocity is used as the convective velocity, and conversely, in regions where $u' > 0$, signals are compressed. In order to obtain the true spatial signal, the local velocity must be used as the convective velocity (this is already justified in § 2.1, see also § 3.3 for the physical reasoning). For a signal that is equally spaced in time, invoking Taylor's hypothesis and using $\langle u \rangle$ as the convective velocity leads to an evenly spaced

https://doi.org/10.1017/jfm.2017.803 Published online by Cambridge University Press

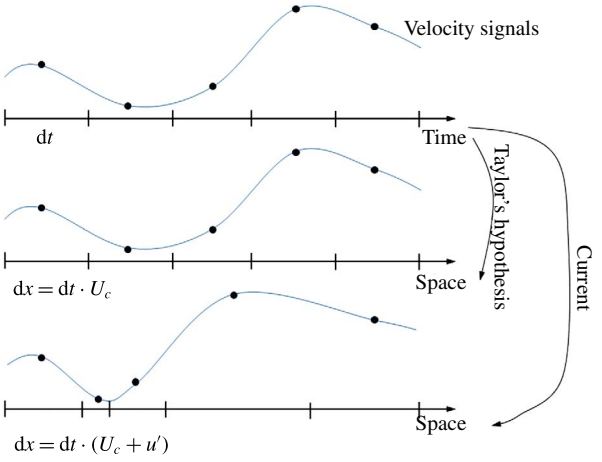


FIGURE 7. (Colour online) A schematic of the proposed scheme to convert temporal velocity signals to spatial signals. Instead of using the mean velocity as the convective velocity (Taylor's hypothesis), the local fluid velocity is used.

spatial signal with the spatial resolution $\mathrm{d}x = \mathrm{d}t \cdot \langle u \rangle$. On the other hand, using the local velocity as the local convective velocity,

$$u_c = \langle u \rangle + u' = u, \tag{3.1}$$

yields an unevenly spaced signal with $\mathrm{d}x = \mathrm{d}t \cdot (\langle u \rangle + u')$ (see figure 7). In addition to (3.1), Dróżdż & Elsner (2017) proposed a convective velocity that depends on the third-order moments $\langle u'_S u'^2_L \rangle$, and Baars *et al.* (2017) suggested the use of the large-scale velocity as the convective velocity. As will be clear, equation (3.1) suffices for the purpose of this work. Therefore, further complications as suggested in Dróżdż & Elsner (2017) and Baars *et al.* (2017) will not be pursued.

As a first test case, equation (3.1) is applied to the temporal signals obtained from the $u_c = 1$ case in § 2.2. The resulting amplitude modulation strength is $R = 0.083$, which is comparable to the result obtained using the spatial data. In figure 4, a comparison is shown for the one-dimensional advection-diffusion problem between R computed from the temporal data using Taylor's hypothesis, spatial data and temporal data using the proposed scheme in (3.1). As we can see from figure 4, the spatial amplitude modulation is correctly captured using (3.1).

3.2. *Reassessment of amplitude modulation*

We now re-analyse the temporal HW measurements using the proposed scheme (3.1). The effects of amplitude modulation on flow quantities including the premultiplied power spectrum, $\langle u'^2 \rangle$, and $\langle u'^3 \rangle$ are reassessed for the spatial amplitude modulation.

The amplitude modulation R and the parameter β in (1.2) are obtained as follows. First, the temporal signal is converted to the spatial domain using (3.1). Second, a top-hat filter in Fourier space is applied to the converted signal with a cutoff filtering length $l^+ = 4000$; u'_L is the large-scale filtered signal and the small-scale signal u'_S is the complement. The envelope of the small-scale signal is obtained by applying the Hilbert transformation to the small-scale signal (see Mathis *et al.* 2009*a*). Third, the large-scale component of the envelope is obtained by applying a low-pass filter to

https://doi.org/10.1017/jfm.2017.803 Published online by Cambridge University Press

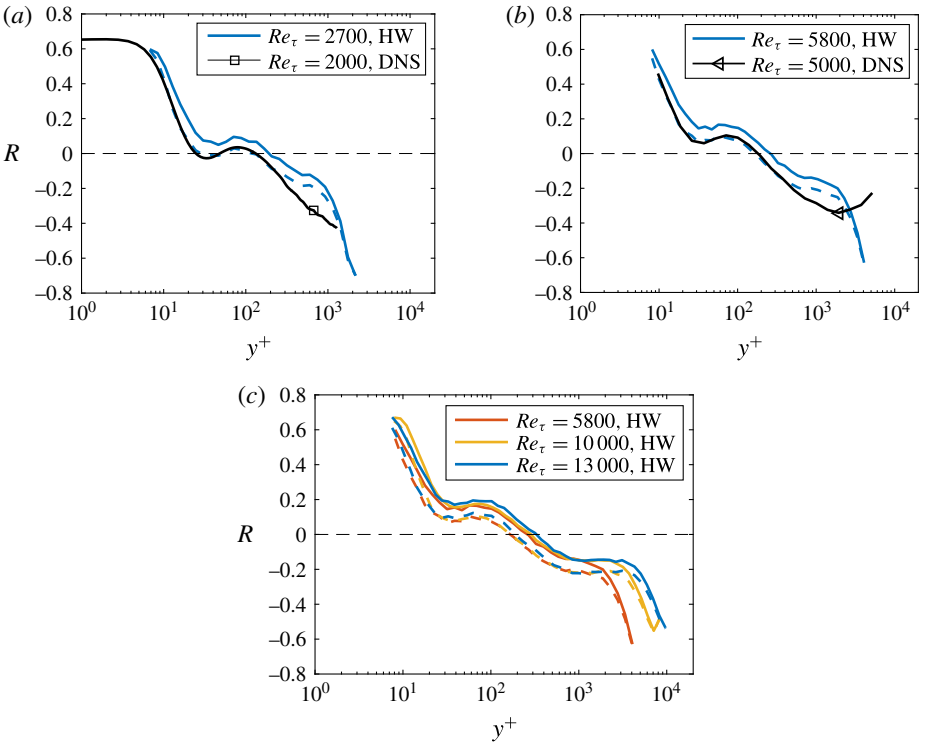


FIGURE 8. (Colour online) (*a*) Amplitude modulation as a function of the wall-normal distance. Taylor's frozen turbulence hypothesis is invoked to obtain the blue solid line, and (3.1) is used to obtain the dashed line. The black bold line is obtained using spatial signals directly from DNS. (*b*) Same as (*a*) but at different Reynolds numbers. (*c*) HW data at three different Reynolds numbers.

$\mathrm{env}(u'_S)$ with the cutoff length scale of $l^+ = 4000$. After $\mathrm{env}_L(u'_S)$ and u'_L are obtained, R is computed according to (1.1). Fourth, β is computed such that $\langle \mathrm{env}_L(u^*) \cdot u'_L \rangle = 0$. This procedure will also yield the de-modulated signal u^* (according to (1.2)). The procedure for calculating R and the de-modulated signals using DNS data is similar, except that both R and β are averaged in the spanwise direction.

Figure 8 shows the amplitude modulation as a function of the wall-normal distance. Both Taylor's hypothesis and (3.1) are used to process the HW data. A few observations can be made. First, when (3.1) is applied, R reduces by ≈ 0.1 within $30 < y^+ < 100$. Second, the HW results follow the DNS results at similar Reynolds numbers when the local fluid velocity is used as the local convective velocity. Third, amplitude modulation is still an increasing function of the Reynolds number (at a fixed y^+ location), although beyond $Re_\tau = 5200$, the dependence on Reynolds number becomes weak and R remains at ≈ 0.1 in the buffer layer. Fourth, within some wall-normal distances, temporal modulation and spatial modulation differ in sign, therefore the presence of temporal modulation does not necessarily guarantee the presence of spatial modulation and *vice versa*. Fifth, according to figure 8(*c*), the extent of the region within which spatial amplitude modulation is positive is independent of Re_τ, whereas for temporal modulation, the extent of this region increases as a function of Re_τ. Those observations suggest that the significance of

https://doi.org/10.1017/jfm.2017.803 Published online by Cambridge University Press

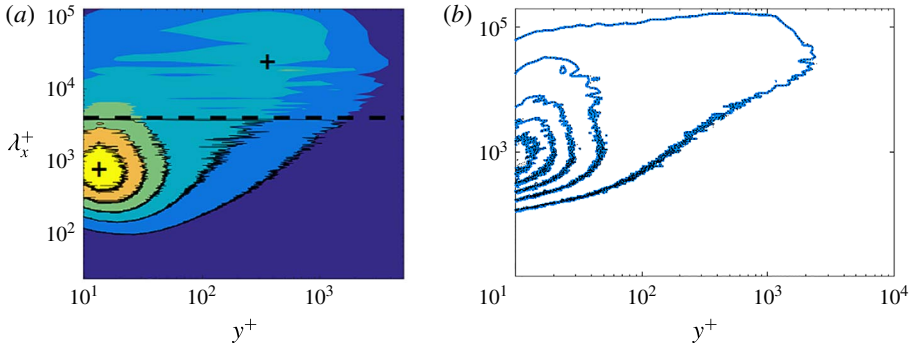


FIGURE 9. (Colour online) (*a*) Premultiplied power spectra of DNS channel flow at $Re_\tau = 5200$ (colour contours). The approximate location of the inner and outer peaks are indicated using '+'. The lines are the same contour levels but for u^*, which is defined in (1.2). The filtering length scale is $l^+ = 4000$ and is denoted with the dashed black line. (*b*) Premultiplied power spectra of the streamwise velocity fluctuation for the $Re_\tau = 13\,000$ HW boundary layer data. Five evenly spaced contour levels are plotted. The exact magnitudes of the spectra are not relevant here. Blue lines are for the full signal $u'_S + u'_L$ and the black lines are for the de-modulated signals $u^* + u'_L$, where only superposition is accounted for.

amplitude modulation has been over-estimated, and spatial amplitude modulation is an important physical flow mechanism only for $y^+ \lesssim O(100)$ at high Re_τ. At a sufficiently high Reynolds numbers, amplitude modulation might be a significant physical process that one must account for in the modelling of fluid motions in the buffer layer, but the Reynolds number at which these considerations must be made are higher than previously reported (i.e. $Re_\tau \approx 1000$, Mathis *et al.* (2013)).

The importance of temporal amplitude modulation has been examined by comparing the premultiplied streamwise power spectra of the full velocity signal and the de-modulated signal (1.2) (see e.g. Mathis *et al.* 2011*a*, 2009*a*). Here we repeat the analysis for spatial modulation. In figure 9(*a*) we compare the premultiplied spectra of u'_S and u^* using DNS of channel flow at $Re_\tau = 5200$. At this Reynolds number, the premultiplied spectra of the de-modulated signal u^* and the full small-scale signal u'_S are not tellingly different. Figure 9(*b*) shows the premultiplied spectrum of $u' = u'_S + u'_L$ and $u^* + u'_L$. The premultiplied spectrum of the full signal is again not significantly different from the de-modulated signal, suggesting that the spatial amplitude modulation process is not a physically significant process for the power spectrum. This is consistent with Mathis *et al.* (2011*a*), where the same analysis was done for the temporal data.

Similar conclusions exist for the variance of the streamwise velocity fluctuations, for which $\langle (u'_S + u'_L)^2 \rangle \approx \langle (u^* + u'_L)^2 \rangle$ (not shown). Figure 10 shows $\langle (u_S + u_L)^3 \rangle$ and $\langle (u^* + u_L)^3 \rangle$ as functions of the wall-normal distance for flows at friction Reynolds numbers $Re_\tau = 2700$ and $Re_\tau = 13\,000$. The skewness of the de-modulated signal is below that of the full signal in the near-wall region and above the skewness of the full signal in the bulk region, which is in contrast with Mathis *et al.* (2011*a*), where the third-order moment of the de-modulated signal is consistently smaller than that of the full signal. Although there is no direct evidence, the difference between the temporally and spatially de-modulated skewness are likely because of the shift in the y^+ location of the zero crossing of R. As for the effect of the Reynolds number, the difference

https://doi.org/10.1017/jfm.2017.803 Published online by Cambridge University Press

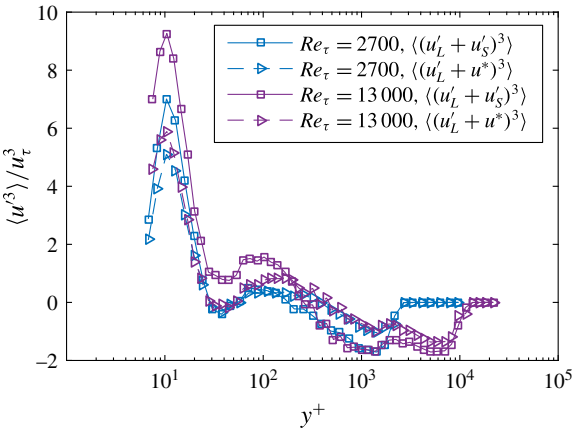


FIGURE 10. (Colour online) $\langle (u'_S + u'_L)^3 \rangle$ and $\langle (u^* + u'_L)^3 \rangle$ as functions of the wall-normal distance for $Re_\tau = 2700$ and $Re_\tau = 13\,000$.

between the de-modulated signal and the full signal increases as the Reynolds number increases, as noted in Mathis *et al.* (2011*a*).

3.3. *Spatial and temporal amplitude modulation*

Based on the results in §§ 2 and 3.2, we may conclude that (3.1) must be employed if temporal HW data are to be used to study spatial amplitude modulation. It is clear from § 2.1 that Taylor's hypothesis cannot be used for studying spatial amplitude modulation because it distorts spatial fluid structures. However, it is not clear why distorting fluid structures in space would affect measurements of spatial amplitude modulation. In this section, we briefly discuss the physical rationale behind (3.1) and the distinction between temporal and spatial amplitude modulation. As discussed in Chernyshenko, Marusic & Mathis (2012), Agostini & Leschziner (2014), Zhang & Chernyshenko (2016) and Baars *et al.* (2017), at sufficiently high Reynolds numbers where the small scales are well separated from the large scales in the power spectrum, the small scales are subjected to the large-scale fluctuations in the wall shear stresses. These shear stresses are modulated by the large-scale velocity fluctuations. Since the near-wall cycle scales with the inner units, it is then expected that in regions where the wall shear stresses are high, the near-wall turbulence would be more agitated due to an increase in the local friction velocity; and the near-wall turbulence would be subdued in regions where the wall shear stresses are small. In light of this interpretation of amplitude modulation, if temporal signals are to be used to study spatial amplitude modulation, one must scale $\mathrm{d}t$ (the sampling time step) using the local viscous scales. With a given temporal resolution in absolute units (e.g. seconds), $\mathrm{d}t$ represents a slightly larger temporal span in regions where the friction velocity is high, and a slightly smaller temporal span in regions where the friction velocity is low. The local temporal resolution can be estimated as

$$\mathrm{d}t_l^+ = \frac{(\langle \tau_w \rangle + \tau'_w)\mathrm{d}t}{\rho \nu} \approx \frac{\langle \tau_w \rangle \mathrm{d}t}{\rho \nu} \left(1 + \frac{\tau'_w}{\langle \tau_w \rangle}\right) \approx \mathrm{d}t^+ \left(1 + \frac{\tau'_w}{\langle \tau_w \rangle}\right), \tag{3.2}$$

where $\mathrm{d}t_l^+$ is the temporal resolution measured using local viscous units and τ'_w is the fluctuation in the local wall shear stress. If we can assume the fluctuations in wall

https://doi.org/10.1017/jfm.2017.803 Published online by Cambridge University Press

shear stresses and the near-wall velocity fluctuations are well correlated (Agostini & Leschziner 2014; Talluru *et al.* 2014; Baars *et al.* 2017), then

$$\frac{\tau_w'}{\langle \tau_w \rangle} \propto \frac{u'}{\langle u \rangle}. \tag{3.3}$$

Equations (3.2) and (3.3) then directly lead to a convective velocity

$$u_c = \langle u \rangle + \text{Const. } u', \tag{3.4}$$

where Const. is an $O(1)$ constant. This is the physical justification for (3.1). We have used Const. $= 1$ for the present study which has proved to be sufficient. Hence (3.1) is justified both from an *a posteriori* sense and from an *a priori* sense.

4. Conclusions

Amplitude and frequency modulation in wall-bounded turbulence have so far received significant attention, including several attempts to incorporate these near-wall physics into LES wall models (Sidebottom *et al.* 2014; Park *et al.* 2016) and in resolvent analysis (McKeon 2017). The significance of amplitude modulation in the near-wall region ($30 \lesssim y^+ \lesssim 100$) has, however, been largely over-stated due to the use of a global convective velocity for fluid motions of all scales. The application of Taylor's hypothesis with a global convective velocity leads to an over-prediction of amplitude modulation of up to 200 % in the buffer layer (previous analysis may be considered as for the temporal amplitude modulation). Here, in order to properly characterize the spatial amplitude modulation using experimental temporal measurements, we propose to use the local fluid velocity instead of the mean velocity as the convective velocity. The effects of amplitude modulation are then reassessed. Among the few flow quantities investigated here including the premultiplied power spectrum, $\langle u'^2 \rangle$ and $\langle u'^3 \rangle$, amplitude modulation is still only relevant for the skewness. Since R is not an independent measure of amplitude modulation but also a measure of the skewness (Schlatter & Örlü 2010; Mathis *et al.* 2011*b*), the usefulness of the amplitude modulation process is yet to be consolidated. In other words, a flow quantity that is not a direct measure of amplitude modulation but depends critically on the modulation process is yet to be found. Other than the phenomenology, the flow physics behind amplitude modulation remain to be explored. The full Navier–Stokes equations are a difficult system to study in order to characterize modulation from a theoretical point of view. The 1-D advection-diffusion equation, which also leads to amplitude modulation, may provide a path to unravel the physics behind the modulation process.

Acknowledgements

X.I.A.Y. is funded by the US AFOSR, grant no. 1194592-1-TAAHO monitored by Dr I. Leyva. M.F.H. is funded through the National Science Foundation Graduate Research Fellowship under grant no. DGE-1656518 and the Stanford Graduate Fellowship. The authors would like to acknowledge P. Moin, I. Marusic, W. Baars, C. Meneveau and A. Lozano-Duran for their generous help and fruitful discussions. We would also like to acknowledge M. Lee for making the DNS data available and E. L. Holzbaur for the thoughtful comments on the manuscript.

https://doi.org/10.1017/jfm.2017.803 Published online by Cambridge University Press

REFERENCES

AGOSTINI, L. & LESCHZINER, M. A. 2014 On the influence of outer large-scale structures on near-wall turbulence in channel flow. *Phys. Fluids* **26** (7), 075107.

BAARS, W. J., HUTCHINS, N. & MARUSIC, I. 2017 Reynolds number trend of hierarchies and scale interactions in turbulent boundary layers. *Phil. Trans. R. Soc. Lond.* A **375** (2089), 20160077.

BAARS, W. J., TALLURU, K. M., HUTCHINS, N. & MARUSIC, I. 2015 Wavelet analysis of wall turbulence to study large-scale modulation of small scales. *Exp. Fluids* **56** (10), 188.

BANDYOPADHYAY, P. R. & HUSSAIN, A. 1984 The coupling between scales in shear flows. *Phys. Fluids* **27** (9), 2221–2228.

CHERNYSHENKO, S. I., MARUSIC, I. & MATHIS, R. 2012 Quasi-steady description of modulation effects in wall turbulence. arXiv:1203.3714.

CHOI, H. & MOIN, P. 2012 Grid-point requirements for large eddy simulation: Chapman's estimates revisited. *Phys. Fluids* **24** (1), 011702.

DEL ÁLAMO, J. C. & JIMÉNEZ, J. 2009 Estimation of turbulent convection velocities and corrections to Taylor's approximation. *J. Fluid Mech.* **640**, 5–26.

DEL ALAMO, J. C., JIMÉNEZ, J., ZANDONADE, P. & MOSER, R. D. 2004 Scaling of the energy spectra of turbulent channels. *J. Fluid Mech.* **500**, 135–144.

DORON, P., BERTUCCIOLI, L., KATZ, J. & OSBORN, T. R. 2001 Turbulence characteristics and dissipation estimates in the coastal ocean bottom boundary layer from PIV data. *J. Phys. Oceanogr.* **31** (8), 2108–2134.

DRÓŻDŻ, A. & ELSNER, W. 2017 Amplitude modulation and its relation to streamwise convection velocity. *Intl J. Heat Fluid Flow* **63**, 67–74.

GANAPATHISUBRAMANI, B., HUTCHINS, N., MONTY, J. P., CHUNG, D. & MARUSIC, I. 2012 Amplitude and frequency modulation in wall turbulence. *J. Fluid Mech.* **712**, 61–91.

GENG, C., HE, G., WANG, Y., XU, C., LOZANO-DURÁN, A. & WALLACE, J. M. 2015 Taylor's hypothesis in turbulent channel flow considered using a transport equation analysis. *Phys. Fluids* **27** (2), 025111.

HOYAS, S. & JIMÉNEZ, J. 2006 Scaling of the velocity fluctuations in turbulent channels up to $Re_\tau = 2003$. *Phys. Fluids* **18** (1), 011702.

HULTMARK, M., VALLIKIVI, M., BAILEY, S. C. C. & SMITS, A. J. 2012 Turbulent pipe flow at extreme Reynolds numbers. *Phys. Rev. Lett.* **108** (9), 094501.

HUTCHINS, N. & MARUSIC, I. 2007 Large-scale influences in near-wall turbulence. *Phil. Trans. R. Soc. Lond.* A **365** (1852), 647–664.

HUTCHINS, N., NICKELS, T. B., MARUSIC, I. & CHONG, M. 2009 Hot-wire spatial resolution issues in wall-bounded turbulence. *J. Fluid Mech.* **635**, 103–136.

KIM, J. & HUSSAIN, F. 1993 Propagation velocity of perturbations in turbulent channel flow. *Phys. Fluids* **5** (3), 695–706.

LEE, M., MALAYA, N. & MOSER, R. D. 2013 Petascale direct numerical simulation of turbulent channel flow on up to 786k cores. In *Proceedings of the International Conference on High Performance Computing, Networking, Storage and Analysis*, p. 61. ACM.

LEE, M. & MOSER, R. D. 2015 Direct numerical simulation of turbulent channel flow up to $Re_\tau \approx 5200$. *J. Fluid Mech.* **774**, 395–415.

LOZANO-DURÁN, A. & JIMÉNEZ, J. 2014*a* Effect of the computational domain on direct simulations of turbulent channels up to $Re_\tau = 4200$. *Phys. Fluids* **26** (1), 011702.

LOZANO-DURÁN, A. & JIMÉNEZ, J. 2014*b* Time-resolved evolution of coherent structures in turbulent channels: characterization of eddies and cascades. *J. Fluid Mech.* **759**, 432–471.

MARUSIC, I., MATHIS, R. & HUTCHINS, N. 2010 Predictive model for wall-bounded turbulent flow. *Science* **329** (5988), 193–196.

MARUSIC, I., MONTY, J. P., HULTMARK, M. & SMITS, A. J. 2013 On the logarithmic region in wall turbulence. *J. Fluid Mech.* **716**, R3.

MATHIS, R., HUTCHINS, N. & MARUSIC, I. 2009*a* Large-scale amplitude modulation of the small-scale structures in turbulent boundary layers. *J. Fluid Mech.* **628**, 311–337.

MATHIS, R., HUTCHINS, N. & MARUSIC, I. 2011*a* A predictive inner-outer model for streamwise turbulence statistics in wall-bounded flows. *J. Fluid Mech.* **681**, 537–566.

https://doi.org/10.1017/jfm.2017.803 Published online by Cambridge University Press

MATHIS, R., MARUSIC, I., CHERNYSHENKO, S. I. & HUTCHINS, N. 2013 Estimating wall-shear-stress fluctuations given an outer region input. *J. Fluid Mech.* **715**, 163.

MATHIS, R., MARUSIC, I., HUTCHINS, N. & SREENIVASAN, K. 2011*b* The relationship between the velocity skewness and the amplitude modulation of the small scale by the large scale in turbulent boundary layers. *Phys. Fluids* **23** (12), 121702.

MATHIS, R., MONTY, J. P., HUTCHINS, N. & MARUSIC, I. 2009*b* Comparison of large-scale amplitude modulation in turbulent boundary layers, pipes, and channel flows. *Phys. Fluids* **21** (11), 111703.

MCKEON, B. 2017 The engine behind (wall) turbulence: perspectives on scale interactions. *J. Fluid Mech.* **817**, doi:10.1017/jfm.2017.115.

MOIN, P. 2009 Revisiting Taylor's hypothesis. *J. Fluid Mech.* **640**, 1–4.

PARK, G., HOWLAND, M. F., LOZANO-DURAN, A. & MOIN, P. 2016 Prediction of wall shear-stress fluctuations in wall-modeled large-eddy simulation. In *APS Meeting Abstracts*.

PIOMELLI, U. & BALARAS, E. 2002 Wall-layer models for large-eddy simulations. *Annu. Rev. Fluid Mech.* **34** (1), 349–374.

RAO, K. N., NARASIMHA, R. & NARAYANAN, M. A. B. 1971 The 'bursting' phenomenon in a turbulent boundary layer. *J. Fluid Mech.* **48** (02), 339–352.

SCHLATTER, P. & ÖRLÜ, R. 2010 Quantifying the interaction between large and small scales in wall-bounded turbulent flows: a note of caution. *Phys. Fluids* **22** (5), 051704.

SIDEBOTTOM, W., CABRIT, O., MARUSIC, I., MENEVEAU, C., OOI, A. & JONES, D. 2014 Modelling of wall shear-stress fluctuations for large-eddy simulation. In *Proc. 19th Australasian Fluid Mechanics Conf., Melbourne, Australia*.

SQUIRE, D. T., HUTCHINS, N., MORRILL-WINTER, C., SCHULTZ, M. P., KLEWICKI, J. C. & MARUSIC, I. 2017 Applicability of Taylor's hypothesis in rough- and smooth-wall boundary layers. *J. Fluid Mech.* **812**, 398–417.

TALLURU, K. M., BAIDYA, R., HUTCHINS, N. & MARUSIC, I. 2014 Amplitude modulation of all three velocity components in turbulent boundary layers. *J. Fluid Mech.* **746**, R1.

TAYLOR, G. I. 1938 The spectrum of turbulence. *Proc. R. Soc. Lond.* A **164**, 476–490.

YANG, X. I. A., MARUSIC, I. & MENEVEAU, C. 2016*a* Hierarchical random additive process and logarithmic scaling of generalized high order, two-point correlations in turbulent boundary layer flow. *Phys. Rev. Fluids* **1** (2), 024402.

YANG, X. I. A., MARUSIC, I. & MENEVEAU, C. 2016*b* Moment generating functions and scaling laws in the inertial layer of turbulent wall-bounded flows. *J. Fluid Mech.* **791**, R2.

YANG, X. I. A., MENEVEAU, C., MARUSIC, I. & BIFERALE, L. 2016*c* Extended self-similarity in moment-generating-functions in wall-bounded turbulence at high Reynolds number. *Phys. Rev. Fluids* **1** (4), 044405.

ZAMAN, K. B. M. Q. & HUSSAIN, A. K. M. F. 1981 Taylor hypothesis and large-scale coherent structures. *J. Fluid Mech.* **112**, 379–396.

ZHANG, C. & CHERNYSHENKO, S. I. 2016 Quasisteady quasihomogeneous description of the scale interactions in near-wall turbulence. *Phys. Rev. Fluids* **1** (1), 014401.

https://doi.org/10.1017/jfm.2017.803 Published online by Cambridge University Press